Domain of oscillatory growth in directional solidification of dilute binary alloys

Evgenia Babushkina, Nicholas M. Bessonov, and Alexander L. Korzhenevskii
Institute for Problems of Mechanical Engineering, RAS, Bol'shoi prospect, V. O., 61, St. Petersburg 199178, Russia

Richard Bausch
Institut für Theoretische Physik IV, Heinrich-Heine-Universität Düsseldorf, Universitätsstrasse 1, D-40225 Düsseldorf, Germany

Rudi Schmitz
Institut für Theoretische Festkörperphysik, RWTH Aachen University, Templergraben 55, D-52056 Aachen, Germany
(Received 14 January 2013; published 10 April 2013)

The oscillatory growth of a dilute binary alloy has recently been described by a nonlinear oscillator equation that applies to small temperature gradients and large growth velocities in the setup of directional solidification. Based on a one-dimensional stability analysis of stationary solutions of this equation, we explore in the present paper the complete region where the solidification front propagates in an oscillatory way. The boundary of this region is calculated exactly, and the nature of the oscillations is evaluated numerically in several segments of the region.

DOI: 10.1103/PhysRevE.87.042402 PACS number(s): 81.10.Aj, 68.35.Dv, 05.70.Np

I. INTRODUCTION

The frequently observed periodic layering structures in dilute binary alloys are generated by oscillatory growth from a melt in the setup of directional solidification [1]. Theoretical explanations of this mechanism have used a phenomenological approach [1], a diffusion equation with nonequilibrium boundary conditions [2], or simulations, based on a phase-field model [3].

We recently described the oscillatory propagation of a planar solidification front by a nonlinear oscillator equation, which we have derived [4] from a previously established capillary-wave representation of a phase-field model [5]. This oscillator equation only applies to small values of the temperature gradient and to velocities of the solidification front in the rapid-growth regime where most of the layering structures have been observed. In order to explore the possibility of interface oscillations at arbitrary values of the temperature gradient and of the growth velocity, we have to go back to the level of an integro-differential equation.

As a first step we consider solutions of this equation that describe steady-state motions of the interface. We then perform a one-dimensional linear stability analysis of these solutions, thereby disregarding deformations of the planar interface. The remaining nonuniform interface motions constitute an instability similar to that found by Cahn in grain-boundary motion [6], and, in the present case, they initiate the interface oscillations. In the plane, spanned by the temperature gradient and the average growth velocity, the Cahn instability occurs in a tongue-like area. For the model considered in the present paper, we have exactly calculated the contour of this tongue. Fragments of the contour have been discussed in the low- and large-velocity regimes in Ref. [7] and at some fixed value of the temperature gradient in Ref. [8].

The procedure in Ref. [7] was intended to readjust the earlier stability analysis in Ref. [9] by founding it on the semiphenomenological approach, presented in Ref. [10], and on an unsettled generalization of the Gibbs-Thomson relation. Reference [8] instead relies on a numerical evaluation of a well-established phase-field model.

The result of our exact calculation complements the description of the similar-looking tongue of the Mullins-Sekerka instability [11]. This tongue has been calculated in Ref. [12] and measured in Ref. [13] for a moving nematic-isotropic interface. The Mullins-Sekerka instability initiates the formation of cellular and dendritic interface deformations, and by the mechanism described in Ref. [4], contributes to the formation of the frequently observed banded structures in metallic alloys [1].

In order to explore the possible existence of oscillatory solutions of the integro-differential equation, we have to resort to numerical evaluations. From these calculations it turns out that oscillations, in fact, continue to exist and qualitatively look similar to those previously found in Ref. [4]. In accordance with the results of our stability analysis, oscillatory solutions are only observed within a finite velocity interval. On approaching the lower limit of this interval, the propagating interface progressively shows the behavior of relaxation oscillations. In further agreement with the stability analysis, oscillations of the interface do not exist above some critical value of the temperature gradient.

II. PLANAR INTERFACE PROPAGATION

As in Ref. [4], we exclusively consider the propagation of a planar solidification front, which is described by the dimensionless model equations

$$\begin{aligned} H &= \frac{\gamma}{2}\int_{-\infty}^{+\infty} dz\,[C(z,t)-U(z-Z(t))]^2, \\ \partial_t Z &= p\left(F-\frac{\delta H}{\delta Z}\right), \quad \partial_t C = \partial_z^2\,\frac{1}{\gamma}\,\frac{\delta H}{\delta C}, \\ F &= F_P - m^2[Z(t)-v_P\,t] \end{aligned} \tag{1}$$

for the the interface position $Z(t)$ and the solute excess concentration $C(z,t)$ relative to its value $C_S \equiv 1$ in the solid

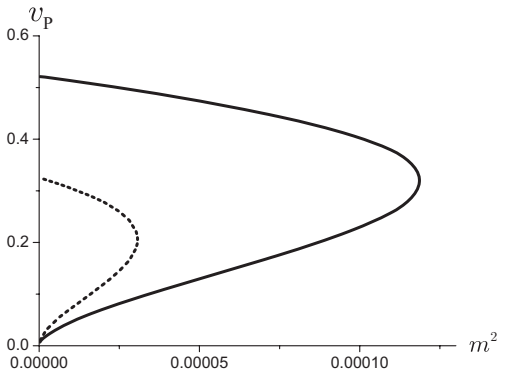

FIG. 1. Neutral stability lines in the m^2, v_P plane for $p = 100$, $\gamma = 0.01$ (solid line), and $\gamma = 0.007$ (dotted line).

phase. The parameter γ measures the miscibility gap $\Delta C = C_L - C_S$, where C_L is the solute density in the liquid phase, all concentrations referring to some fixed temperature T_S. Another input quantity of the model is the function $U(z - Z)$, which describes the equilibrium-concentration profile of the solute at T_S. The parameter p measures the mobility of the interface, and F is the driving force, involving the externally controlled values of the temperature gradient m^2 and of the pulling velocity v_P. The value of F_P is fixed by the stationary solutions $Z_P(t) = v_P t, C_P(z - v_P t)$ of the equations of motion in Eqs. (1).

The equations of motion have the explicit form

$$\frac{1}{p}\dot{Z}(t) = F_P - m^2[Z(t) - v_P t] - \gamma \int_{-\infty}^{+\infty} dz \times U'(z - Z(t))[C(z,t) - U(z - Z(t))],$$
$$\left(\partial_t - \partial_z^2\right)C(z,t) = -U''(z - Z(t)), \tag{2}$$

and in the stationary case reduce to

$$\frac{1}{p} v_P = F_P - \gamma \int_{-\infty}^{+\infty} d\zeta\, U'(\zeta)[C_P(\zeta) - U(\zeta)],$$
$$\left(\partial_\zeta^2 + v\partial_\zeta\right)C_P(\zeta) = U''(\zeta). \tag{3}$$

For steady-state boundary conditions

$$C_P(+\infty) = C_P(-\infty) = 0, \tag{4}$$

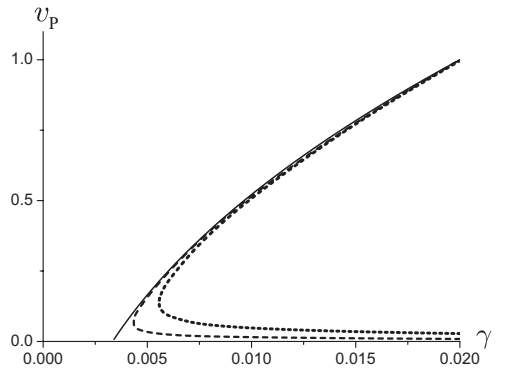

FIG. 2. Neutral stability lines in the γ, v_P, plane for $p = 100$, and for $m^2 = 0$ (solid line), $m^2 = 1 \times 10^{-6}$ (dashed line), and $m^2 = 9 \times 10^{-6}$ (dotted line).

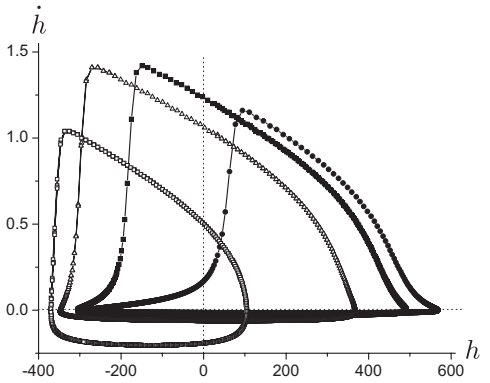

FIG. 3. Limit cycles in the $h, \dot{h}$ phase space for $p = 100$, $m^2 = 9 \times 10^{-6}$, $\gamma = 10^{-2}$, and, from left to right, decreasing pulling velocities $v_P = 0.3, v_P = 0.1, v_P = 0.05, v_P = 0.03$.

the second equation in Eqs. (3) has the solution

$$C_P(\zeta; v_P) = \int_{-\infty}^{\zeta} d\zeta'\, U'(\zeta') \exp[v_P(\zeta' - \zeta)], \tag{5}$$

which, after insertion into the first equation in Eqs. (3), determines the value of F_P.

By subtracting Eqs. (3) from Eqs. (2) one obtains for the displacements

$$h(t) \equiv Z(t) - v_P t, \quad c(\zeta,t) \equiv C(\zeta + Z(t),t) - C_P(\zeta), \tag{6}$$

the coupled equations

$$\left(\frac{1}{p}\partial_t + m^2\right) h(t) = -\gamma \int_{-\infty}^{+\infty} d\zeta\, U'(\zeta) c(\zeta,t),$$
$$\left\{\partial_t - [v_P + \dot{h}(t)]\partial_\zeta - \partial_\zeta^2\right\} c(\zeta,t) = C_P'(\zeta)\dot{h}(t). \tag{7}$$

This form of the equations is especially convenient for numerical evaluations, as the only nonlinear coupling between the variables $h(t)$ and $c(\zeta,t)$ is localized in the third term of the second line in Eqs. (7). If the solution $c(\zeta,t)$ of the latter equation is inserted into the first line in Eqs. (7), one arrives at an integro-differential equation for $h(t)$.

In order to obtain quantitative expressions for $h(t)$ and $c(\zeta,t)$, we now adopt the specific model

$$U(\zeta) = \Theta(-\zeta)\exp(\zeta) + \Theta(\zeta)[2 - \exp(-\zeta)], \tag{8}$$

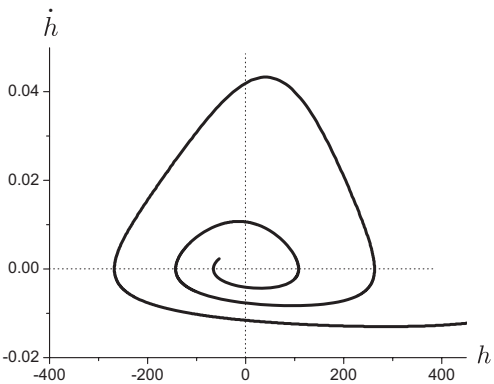

FIG. 4. Oscillatory approach of the fixed point $h = \dot{h} = 0$ for the same parameter values as in Fig. 3, but $v_P = 0.025$.

derived in Ref. [5] from a double-parabola phase-field model. Then, Eq. (5) yields

$$C_P(\zeta) = \Theta(-\zeta)\frac{\exp(\zeta)}{1+v_P} + \Theta(\zeta)\left[\frac{2\exp(-v_P\zeta)}{1-v_P^2} - \frac{\exp(-\zeta)}{1-v_P}\right] \tag{9}$$

so that all input quantities in Eqs. (7) are known.

III. STABILITY OF THE STEADY-STATE PROPAGATION

As a first application, Eqs. (7) allow us to perform a linear stability analysis of the steady-state solutions $Z_P(t), C_P(\zeta,t)$ by dropping the term $\dot{h}(t)\partial_\zeta c(\zeta,t)$. The resulting equations have eigensolutions of the form

$$h(t) = \hat{h}(\omega)\exp(\omega t), \quad c(\zeta,t) = \rho(\zeta,\omega)\hat{h}(\omega)\exp(\omega t), \tag{10}$$

giving rise to the relations

$$\left[\frac{\omega}{p} + m^2 + \gamma g(\omega)\right]\hat{h}(\omega) = 0,$$
$$g(\omega) \equiv \int_{-\infty}^{+\infty} d\zeta\, U'(\zeta)\rho(\zeta,\omega), \tag{11}$$
$$\left(\partial_\zeta^2 + v_P\partial_\zeta - \omega\right)\rho(\zeta,\omega) = -\omega C_P'(\zeta).$$

The solvability condition

$$\frac{\omega}{p} + m^2 + \gamma g(\omega) = 0, \tag{12}$$

finally, determines the generally complex variable ω as a function of the parameters m^2, γ, and v_P.

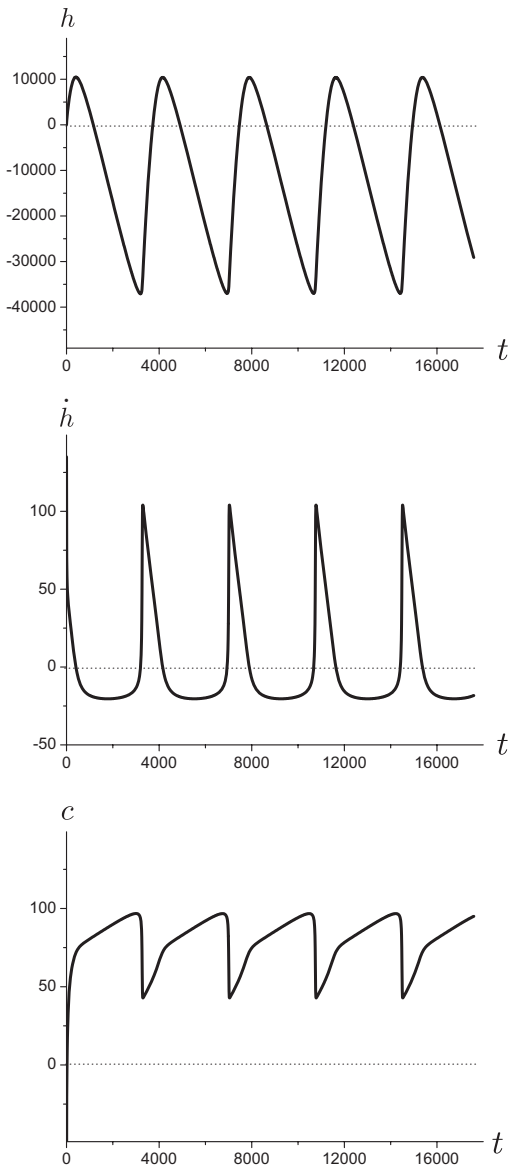

FIG. 5. Trajectories $h(t), \dot{h}(t)$, and $c(0,t)$ for $p = 100$, $\gamma = 10^{-2}$, $m^2 = 9 \times 10^{-6}$, and $v_P = 0.3$.

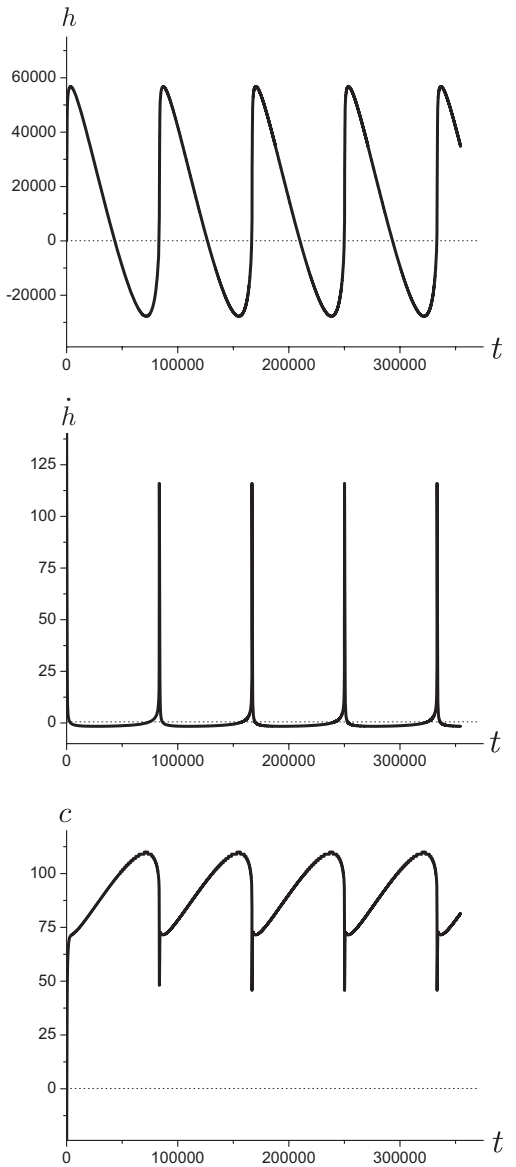

FIG. 6. Trajectories $h(t)$, $\dot{h}(t)$, and $c(0,t)$ for the same parameter set as in Fig. 5, except for the smaller value $v_P = 0.03$ of the pulling velocity.

Evaluation of the last two equations in Eqs. (11) for the model (7) leads to the result

$$g(\omega) = \frac{1}{(1+v_P)^2} - \frac{1}{1+2\lambda}\left[\frac{v_P+\lambda}{(1+v_P+\lambda)^2} + \frac{\lambda}{(1\pm\lambda)^2}\right], \quad \mathrm{Re}(\lambda) \gtrless 0, \tag{13}$$

involving the characteristic root

$$\lambda \equiv -(v_P/2) + \sqrt{(v_P/2)^2+\omega}. \tag{14}$$

The definition (14) implies the relation

$$\omega = \lambda(\lambda + v_P), \tag{15}$$

which shows that in the complex ω plane the cutting line $\mathrm{Re}(\lambda) = 0$ is a parabola, extending from its cusp position at $\omega = 0$ into the half-plane $\mathrm{Re}(\omega) < 0$. Because the outside region $\mathrm{Re}(\lambda) > 0$ of the parabola includes the unstable regime $\mathrm{Re}(\omega) > 0$, we focus on the result (12), applied to the upper branch of the expression (13).

The resulting equation is in accordance with the dispersion relation, derived in Ref. [4], and, by taking $\mathrm{Re}(\omega) = 0$, determines the neutral-stability manifold.

In Fig. 1 the neutral stability lines are plotted in the m^2, v_P plane for $p = 100$ and for two values of γ. They enclose the regions where interface oscillations can occur. The asymptotic parts of the neutral line for $m^2 \to 0$ are in qualitative agreement with the calculations in Ref. [7]. Since the simulations in Ref. [8] have been performed at some fixed value of the temperature gradient, only two points of the neutral lines can be seen in this work. According to Fig. 1, these points merge at some critical value of the temperature gradient. We mention that this behavior also applies to the similar-looking neutral line of the Mullins-Sekerka instability presented in the review article by Flesselles and colleagues [14].

Figure 2 shows the neutral lines in the γ, v_P plane for the choice $p = 100$ and different values of m^2. In all cases, where $m^2 > 0$, these lines have the same topology as those found in Ref. [7], allowing a regime of stable steady-state interface motion at low pulling velocities. The asymptotic curve for $m^2 \to 0$ is identical to the neutral line $F'(v_P) = 0$ found in Ref. [4] in the regime of rapid directional solidification. As demonstrated by the figure, this asymptotic curve is a good approximation for small temperature gradients at sufficiently large pulling velocities.

IV. OSCILLATORY PROPAGATION

In order to discuss the oscillatory behavior expected to occur in the unstable regime, we evaluate the basic Eqs. (7) numerically, using the tools provided by Ref. [15]. The resulting limit cycles in the $h, \dot{h}$ plane are shown in Fig. 3 for different values of the pulling velocity. With decreasing velocity the cycles become increasingly deformed, indicating progressive relaxation oscillations. At $v_P = 0.025$ the $h, \dot{h}$ trajectory approaches the fixed point $h = \dot{h} = 0$ in an oscillatory way, as shown in Fig. 4. This fixed point represents a stable steady-state interface propagation, as to be expected from Figs. 1 and 2.

Fig. 5 shows the time dependence of the trajectories $h(t), \dot{h}(t)$, and $c(0,t)$ for $p = 100$, $m^2 = 9 \times 10^{-6}$, $\gamma = 10^{-2}$, and $v_P = 0.3$. These trajectories look quite similar to those derived from an approximate nonlinear oscillator equation in Ref. [4]. Reducing the pulling velocity to the value $v_P = 0.03$, one observes that the trajectories show a more pronounced character of relaxation oscillations, as shown in Fig. 6.

The oscillations of the propagating interface position $Z(t)$ are responsible for the formation of solute layers, often observed in experiments. In order to describe this effect, our model should be modified by assuming a space-dependent diffusion coefficient, which is very small in the solid phase and therefore leads to an appreciable lifetime of the layering structure.

V. SUMMARY

The present report provides an exact description of the complete domain where, in the setup of directional solidification, the growth of a dilute binary occurs in an oscillatory way. By a numerical evaluation of the growth equations it also characterizes the types of oscillations at high and low growth rates. It would be interesting to verify these features by experiments similar to those described in Ref. [13].

ACKNOWLEDGMENTS

A.L.K. expresses his gratitude to the University of Düsseldorf for its warm hospitality. This work has been supported by the DFG under Grant No. BA 944/4-1, and by the RFBR under Grant No. N10-02-91332.

[1] M. Carrard, M. Gremaud, M. Zimmermann, and W. Kurz, Acta Metall. Mater. **40**, 983 (1992).
[2] A. Karma and A. Sarkissian, Phys. Rev. Lett. **68**, 2616 (1992); Phys. Rev. E **47**, 513 (1993).
[3] M. Conti, Phys. Rev. E **58**, 2071 (1998); **58**, 6101 (1998).
[4] A. L. Korzhenevskii, R. Bausch, and R. Schmitz, Phys. Rev. Lett. **108**, 046101 (2012); Phys. Rev. E **85**, 021605 (2012).
[5] A. L. Korzhenevskii, R. Bausch, and R. Schmitz, Phys. Rev. E **83**, 041609 (2011).
[6] J. W. Cahn, Acta Metall. **10**, 789 (1962).
[7] G. J. Merchant and S. H. Davis, Acta Metall. Mater. **38**, 2683 (1990).
[8] M. Conti, Phys. Rev. E **56**, R6267 (1997).
[9] S. R. Coriell and R. F. Sekerka, J. Cryst. Growth. **61**, 499 (1983).
[10] M. J. Aziz and W. J. Boettinger, Acta metall. mater. **42**, 527 (1994).
[11] W. W. Mullins and R. F. Sekerka, J. Appl. Phys. **35**, 444 (1964).
[12] B. Caroli, C. Caroli, and B. Roulet, J. Phys. Paris **43**, 1767 (1982).
[13] A. J. Simon and A. Libchaber, Phys. Rev. A **41**, 7090 (1990).
[14] J.-M. Flesselles, A. J. Simon, and A. J. Libchaber, Adv. Phys. **40**, 1 (1997).
[15] J. W. Thomas, *Numerical Partial Differential Equations: Finite Difference Methods* (Springer, Berlin, 1999).